

# 1 Assimilating High-resolution Sea Surface Temperature

## 2 Data Improves the Ocean Forecast Potential in the Baltic 3 Sea

4 Ye Liu<sup>1</sup>, Weiwei Fu<sup>2</sup>

5 1. Swedish Meteorological and Hydrological Institute, Norrköping 60176, Sweden.

6 2. Department of Earth System Science, University of California, Irvine, California, 92697, USA.

7  
8 *Correspondence to:* Ye Liu ([ye.liu@smhi.se](mailto:ye.liu@smhi.se))

9  
10 **Abstract.** We assess the impact of assimilating the satellite sea surface temperature (SST) data on  
11 the Baltic forecast, practically on the forecast of ocean variables related to SST. For this purpose, a  
12 multivariable DA system has been developed based on a Nordic version of the Nucleus for European  
13 Modelling of the Ocean (NEMO-Nordic). We use a local Singular Evolutive Interpolated Kalman  
14 (LSEIK) filter to characterize correlation scales in the coastal regions. High resolution SST from  
15 OSISAF is assimilated to verify the performance of DA system. The assimilation run shows very sta-  
16 ble improvements of the model simulation as compared with both independent and dependent observa-  
17 tions. The SST prediction of NEMO-Nordic is significantly enhanced by the DA system. Tempera-  
18 tures are also closer to observation in the DA system than the model results in the water above 100 m  
19 in the Baltic Sea. In the deeper layers, salinity is also slightly improved. Besides, we find that Sea  
20 level anomaly (SLA) is improved with the SST assimilation. Comparison with independent tide gauge  
21 data show that overall root mean square error (RMSE) is reduced by 1.8% and overall correlation co-  
22 efficient is slightly increased. Moreover, the sea ice concentration forecast is improved considerably in  
23 the Baltic proper, the Gulf of Finland and the Bothnian Sea during the sea ice formation period, re-  
24 spectively.

26

27

## 28 **1. Introduction**

29 Monitoring the marine status of the Baltic Sea with relevant resolution and accuracy is a key  
30 requirement to serve the marine policy for detecting the influence of human activities on the environ-  
31 ment and better understanding the response of ocean to accelerating global climate change. The Baltic  
32 Sea is one of the largest brackish seas in the world. It is a semi-enclosed basin, whose hydrography is  
33 highly variable and influenced by large-scale atmospheric processes and significant influx of freshwa-  
34 ter from rivers runoff and precipitation (Leppäranta and Myrberg, 2009). In addition, the water ex-  
35 change between the North Sea and Baltic Sea through the Danish straits is hindered by shallow topo-  
36 graphic restrictions in the transition zone (Fig. 1).

37 A characteristic feature of numerical forecast in the Baltic Sea is in itself a major challenge  
38 because of complex topography and rich dynamics. A number of ocean forecasting systems for the  
39 Baltic Sea have been developed using hydrological model by operational agencies around this region.  
40 Traditionally, these models have a horizontal resolution of 1–5 km and approximately 20–100 layers  
41 in vertical structure (Omstedt et al. 2014). Due to the geographic location and conditions of the Baltic  
42 Sea, even higher resolutions are often needed to better understand the circulation dynamics. However,  
43 even ocean circulation models with a particularly high spatial resolution (e.g. 1 km) cannot resolve all  
44 dynamically important physical processes in the ocean (Malanotte-Rizzoli and Tziperman, 1996). In  
45 general, the forecast quality for a numerical model depends on initial conditions, boundary conditions  
46 (lateral, open boundaries as well as meteorological forcing and bathymetry) and a robust numerical  
47 model itself. As an operational forecasting agency, the Swedish Meteorological and Hydrological In-  
48 stitute's (SMHI) needs to issue well-informed forecasts and warnings for decision making by other  
49 authorities during e.g. severe weather events, but also to the public. To improve the forecast quality,  
50 the core three-dimensional dynamic model of the SMHI operational forecast system has recently mi-  
51 grated to the Nordic version of the Nucleus for European Modelling of the Ocean (NEMO-Nordic).

52 In additional to model development, an extended observational network has been established by

53 the joint efforts of the countries surrounding the Baltic Sea. The observation platforms include vessels,  
54 buoys, coastal stations, satellite, etc. Specially, the observations from satellite have dominated the  
55 coverage of SST observational networks in the Baltic Sea (She et al. 2007). Among satellite products,  
56 the SST is most popularly and widely used [for](#) the operational forecast, reanalysis or validation of the  
57 model because of both its coverage and properties. SST acts as a medium between atmospheric and  
58 oceanic variations through activation of coupling mechanisms. SST is also a key ocean variable to link  
59 many processes that occur in the upper ocean, for example, air-sea exchange of energy, primary  
60 productivity, and formation of water masses (Tranchant et al., 2008).

61 A realistic forecast of SST is essential to an ocean forecasting system. SST is especially im-  
62 portant for the Baltic Sea that the average water depth is only 56 m and its surface water is directly  
63 related to the bottom water by the mixing in the shallow sub-basins. Recently, the applications of SST  
64 for forecasting and analyzing the status of the North Sea and Baltic Sea have received particular atten-  
65 tion. In the short-term forecast, Losa et al. (2012, 2014) investigated the systematic model uncertain-  
66 ties for forecasting the North and Baltic Seas by assimilating the Advanced Very High Resolution  
67 Radiometer (AVHRR) SST data. Nowicki et al. (2015) applied SST observed from Aqua Moderate  
68 Resolution Imaging Spectroradiometer (MODIS) into 3D coupled ecosystem model of the Baltic Sea  
69 with the Cressman analysis scheme. O’Dea et al. (2016) enhanced the SST prediction skill of the oper-  
70 ational system by assimilating both in-situ data and level 2 SST data provided by the Global Ocean  
71 Data Assimilation Experiment High-Resolution SST (GHRSSST) into a European North-West shelf  
72 operational model. Moreover, SST has been used in the long-term analysis in this region. For instance,  
73 Stramska and Bialogrodzka (2015) analyzed spatial and temporal variability of SST in the Baltic sea  
74 based on 32-years of satellite data, which indicate that there is a statistically significant trend of in-  
75 creasing SST in the entire Baltic sea. However, these long-term SST data haven’t been used to verify  
76 the application of sophisticated DA methods for hydrography model in the Baltic profiles simulation,  
77 especially at the Baltic deep water regions. Another important question is: what amount of satellite  
78 SST can improve long-term forecast of ocean variables related to SST in the Baltic Sea.

79 The objective of this study is to address the impact of assimilating a high resolution SST product  
80 on the forecast of the Baltic Sea, particularly the forecast of SST related variables like sea level and

81 sea ice. It is also the first time that satellite SST from [the Ocean and Sea Ice Satellite Application Fa-](#)  
82 [cility \(OSISAF\)](#) was assimilated into NEMO-Nordic model (NEMO variant for the North Sea and  
83 Baltic Sea). For operational forecast, the SST from OSISAF is the most important dataset in the Baltic  
84 Sea [because it differs from hindcast analyzed product like OSTIA \(Operational SST and Sea Ice Anal-](#)  
85 [ysis\) data. As a level 2 product, the OSISAF SST has both good temporal and spatial coverage in the](#)  
86 [Baltic Sea. As there is no hindcast information included in the OSISAF SST, we are able to assess](#)  
87 [direct impacts of assimilating SST observations.](#) Therefore, exploring the potential of this product is  
88 critically important to further improving the new operational forecast system. In addition, our study  
89 will enrich the reanalysis database of the Baltic Sea. In this study, we use the Singular Evolutive Inter-  
90 polated Kalman (SEIK) filter (Pham, 2001) to account for the model uncertainties arising from a wide  
91 range of spatial and temporal scales (Haines, 2010). One of our focuses is the impact of SST on the  
92 modeled sea level and the sea ice in the Baltic Sea. For the whole Baltic Sea, how the SST assimi-  
93 lation influences the temperature and salinity (T/S) on the different depth is another focus of this study.

94 The outline of the paper is as follows: the model configuration and SEIK scheme are described  
95 in Section 2. An overview of the observations used in this study is presented in Section 3. The imple-  
96 mentation of DA experiment is given in section 4 together with the sampling of ensemble and localiza-  
97 tion. Results are compared with observations for temperature, salinity, sea level [anomaly](#) and sea ice in  
98 Section 5. In this section, the impact of data assimilation on the forecasts is also investigated. Conclu-  
99 sions and discussions are given in section 6.

100

## 101 **2. Methodology**

### 102 **2.1 NEMO-Nordic**

103 NEMO (Nucleus for European Modelling of the Ocean; Madec, 2008) has been set up at SMHI  
104 for the North Sea and the Baltic Sea, a configuration called NEMO-Nordic (Hordoir et al., 2015) (Fig.  
105 1). Open boundaries are implemented in northern North Sea between Scotland and Norway and in the  
106 English Channel between Brittany and Cornwall, respectively (Hordoir et al., 2013). In this study,  
107 NEMO-Nordic employs a horizontal resolution of 2 nautical miles (3.7 km) and 56 vertical levels, and

108 with a vertical resolution of 3 m close to the surface, decreasing to 22 m at the bottom of the deepest  
109 part of the Norwegian trench. NEMO-Nordic uses a fully nonlinear explicit free surface (Adcroft and  
110 Campin, 2004). A bulk formulation is used for the surface boundary condition (Large and Yeager,  
111 2004). The ocean model is coupled to the Louvain-la-Neuve Sea Ice Model (LIM3) sea ice model  
112 (Vancoppenolle et al., 2008) with a constant value of  $10^{-3}$  PSU for the sea-ice salinity. A time-splitting  
113 approach is used to compute a barotropic and a baroclinic mode, as well as the interaction between  
114 them. A Tidal Inversion Model is used to define the barotropic mode at the open boundary conditions  
115 (Egbert and Erofeeva, 2002). 11 tidal harmonics are defined for sea level and barotropic tidal veloci-  
116 ties. In addition, a coarse resolution barotropic storm surge model covering a large area of the North-  
117 ern Atlantic basin provides wind-driven sea level that is added to the tidal contribution. The T/S data  
118 at the open boundary are provided by the Levitus climatology (Levitus and Boyer, 1994). Radiation  
119 conditions are applied to calculate baroclinic velocities at these boundaries. A quadratic friction is  
120 applied with a constant bottom roughness of 3 cm, and the drag coefficient is computed for each bot-  
121 tom grid cell. NEMO-Nordic uses a TVD advection scheme with a modified leapfrog approach that  
122 ensures a very high degree of tracer conservation (Leclair and Madec, 2009). Unresolved vertical tur-  
123 bulence is parameterized with  $\kappa$ - $\epsilon$  scheme (Umlauf and Burchard, 2003). In addition, Galperin pa-  
124 rameterization is used to obtain a stable long-term stratification for the Baltic Sea (Galperin et al.,  
125 1988).

126 A Laplacian isopycnal diffusion is used for both momentum and tracers with a diffusion parame-  
127 ter that is constant in time, but varies in space. Additional strong isopycnal diffusion is used close to  
128 the Neva river inflow (Gulf of St. Petersburg) in order to avoid negative salinities. The bottom bound-  
129 ary layer is parameterized to ease the propagation of saltwater inflows between the Danish Straits and  
130 the deepest layers of the Baltic Sea (Beckmann and Doscher, 1997). A free-slip option is used for lat-  
131 eral boundaries.

132 The model is forced by meteorological forcing derived from a downscaled run of Euro4M reanaly-  
133 sis (Dahlgren et al., 2014). The downscaling is based on the regional atmospheric model RCA4 (Sam-  
134 uelsson et al., 2011) which uses the reanalysis data as boundary conditions. A runoff database provides  
135 the river flow to NEMO-Nordic ([Donnelly et al. 2016](#)); it includes inter-annual variability for the Bal-

136 tic Sea basin and is based on climatological values for the North Sea basin. The salinity of the river  
 137 runoff is set to a constant value of  $10^{-3}$  PSU, which is the same value used for the sea-ice to avoid any  
 138 negative salinity.

139

## 140 **2.2 Local Singular Evolutive Interpolated Kalman (LSEIK) filter**

141 The method used to assimilate SST into NEMO-Nordic is the Local Singular Evolutive Interpo-  
 142 lated Kalman (LSEIK) filter (Pham et al., 2001, Nerger et al. 2006). This is a sequential data assimila-  
 143 tion scheme, which is an error subspace extend Kalman filter that uses a minimum number of ensem-  
 144 ble members to reduce the prohibitive computation burden (Pham, 2001). The LSEIK filter proceeds  
 145 in correction and forecast step:

146 1. Forecast: the analysis state  $\mathbf{X}^a$  at time  $t_{i-1}$  is integrated forward to the time of the next available  
 147 observations  $t_i$  to compute the forecast state  $\mathbf{X}^f$ ,

$$148 \quad \mathbf{X}^f(t_i) = \mathbf{M}(t_{i-1}, t_i)\mathbf{X}^a(t_{i-1}) \quad (1),$$

149 where  $\mathbf{M}$  denotes the nonlinear dynamic model operator that integrates a model state from time  $t_{i-1}$   
 150 to time  $t_i$ . The superscript 'f' and 'a' denote the forecast and analysis. The corresponding error covar-  
 151 iance matrix can be expressed as:

$$152 \quad \mathbf{P}^f(t_i) = \mathbf{L}_i[(r + 1)\mathbf{T}^T\mathbf{T}]^{-1}\mathbf{L}_i^T + \mathbf{Q}_i \quad (2),$$

$$153 \quad \mathbf{L}_i = \mathbf{X}^f(t_i)\mathbf{T} \quad (3),$$

154 with  $\mathbf{Q}_i$  being the covariance matrix of model uncertainties and  $r + 1$  is the minimum number of  
 155 sample ensemble members for error covariance matrix. The superscript 'T' denotes the transpose of  
 156 matrix. The full rank matrix  $\mathbf{T}$  has a dimension of  $(r + 1) \times r$  with zero column sums and  $\mathbf{L}$  is a full  
 157 rank  $(r + 1) \times r$  matrix which implicitly represents the model variability.

158 2. Correction: when the observation is available at time  $t_i$ , the LSEIK filter merged the information  
 159 from model and observation to produce the analysis state with the formula:

$$160 \quad \mathbf{X}^a(t_i) = \mathbf{X}^f(t_i) + \mathbf{K}_i[\mathbf{Y}^o(t_i) - \mathbf{H}_i\mathbf{X}^f(t_i)] \quad (4).$$

161 Here  $\mathbf{Y}^o$  is a vector of observations. The gain matrix  $\mathbf{K}$ , which linearly interpolates between the obser-

162 vations and the forecast, is given by

$$163 \quad \mathbf{K}_i = \mathbf{P}_i^f \mathbf{H}_i^T (\mathbf{H}_i \mathbf{P}_i^f \mathbf{H}_i^T + \mathbf{R}_i)^{-1} = \mathbf{L}_i \mathbf{U}_i (\mathbf{H}_i \mathbf{L}_i)^T \mathbf{R}_i^{-1} \quad (5),$$

164 where  $\mathbf{H}_i$  denotes the linearization of observation operator, which mapping the model space to the  
 165 observation space.  $\mathbf{R}$  is the observation error covariance matrix. The matrix  $\mathbf{U}_i$  is updated according to

$$166 \quad \mathbf{U}_i^{-1} = [\mathbf{U}_{i-1} + (\mathbf{L}_i^T \mathbf{L}_i)^{-1} \mathbf{L}_i^T \mathbf{Q}_i \mathbf{L}_i (\mathbf{L}_i^T \mathbf{L}_i)^{-1}]^{-1} + \mathbf{L}_i^T \mathbf{H}_i^T \mathbf{R}_i^{-1} \mathbf{H}_i \mathbf{L}_i \quad (6).$$

167 Localization was used to remove the unrealistic long-range correlation with a quasi-Gaussian  
 168 function and a uniform horizontal correlation scale (Liu et al. 2013). It was performed by neglecting  
 169 observations that were beyond correlation distance from an analyzed grid point. In other words, only  
 170 data located in the “neighborhood” of an analyzed grid point should contribute to the analysis at this  
 171 point(Liu et al. 2009; Janjić et al. 2011).

172 A second-order exact sampling is used to initialize the LSEIK filter. At time  $t_{i-1}$ , a analysis  
 173 state  $\mathbf{X}^a(t_{i-1})$  and its corresponding error covariance matrix  $\mathbf{P}^a(t_{i-1})$ , in the factorized form  
 174  $\mathbf{L}_{i-1} \mathbf{U}_{i-1} \mathbf{L}_{i-1}^T$ , are available. The samples can be given by the following formular:

$$175 \quad \mathbf{X}_k^a(t_{i-1}) = \overline{\mathbf{X}}^a(t_{i-1}) + \sqrt{r+1} \mathbf{L}_{i-1} (\boldsymbol{\Omega}_{k,i-1} \mathbf{C}_{i-1})^T \quad (7).$$

176 For  $1 \leq k \leq r+1$ , the  $\mathbf{C}_{i-1}$  is the Cholesky decomposition of  $\mathbf{U}_{i-1}^{-1}$  and  $\boldsymbol{\Omega}_{i-1}$  is a  $(r+1) \times r$  ma-  
 177 trix with orthonormal columns and zero column sums, where  $\boldsymbol{\Omega}_{k,i-1}$  denotes the  $k^{th}$  row of  $\boldsymbol{\Omega}_{i-1}$ .  $\overline{\mathbf{X}}^a$   
 178 is the average of the analysis state.

### 179 **3. Observations**

#### 180 **3.1 Satellite observations**

181 The satellite SST used in DA was provided by OSISAF (<http://osisaf.met.no/p/sst/index.html>).

182 ~~OSISAF products are using in priority the European Meteorological satellites METEOSAT and~~  
 183 ~~MetOp and also several American satellites operated by NOAA, DMSP and NASA. Its~~ aim is to pro-  
 184 duce, control and distribute operationally in near real-time products using available satellite data. The  
 185 satellite datasets product used here includes the observations from polar orbiting satellites (the EU-  
 186 METSAT MetOp-A and NOAA-18, -19) with the AVHRR instrument. The SST product has a resolu-

187 tion of 5 km and is produced twice daily at 00 UTC and 12 UTC. It covers the Atlantic Ocean from  
188 50°N to 90°N. The SST observations are thermal infrared observations from the AVHRR instrument  
189 and are therefore limited by cloud cover (Kilpatrick et al. 2001). The cloud mask in use is based on a  
190 multi-spectral thresholding algorithm by SMHI. The products were retrieved using a nonlinear split  
191 window algorithm (Walton et al. 1998). The coefficients in the retrieval algorithm are determined  
192 through regression toward in situ observations, and the dataset thus represents the subskin temperature  
193 of the oceans. Further, subskin observations are subject to diurnal warming effects, which can be sig-  
194 nificant in the Baltic Sea. Here only the subskin SST at night ([00 UTC](#)), which is comparable to in situ  
195 (buoy) measurement, is used to minimum this effect. The SST is controlled with the climatology  
196 check. A quality level from 0 to 5 is associated with every pixel. The higher level value, the better the  
197 quality of the observations (Brisson et al., 2001). Observations with quality level 4 (good) or 5 (excel-  
198 lent) are collected for the analysis and low quality observations were removed. By applying the above  
199 quality control processes, only a subset of the original OSISAF products is kept in this study. Based on  
200 the former validation, a bias value of 0.5°C is given for this product.

201 Further, the IceMap from a sea ice concentration dataset with a high spatial resolution of 5 km  
202 ([http://www.smhi.se/oceanografi/iceservice/is\\_prod\\_en.php](http://www.smhi.se/oceanografi/iceservice/is_prod_en.php)) is used to validate the DA results. It is  
203 produced by SMHI and originates from digitized ice charts. An advantage of this data is that the ice  
204 charts are quality checked manually. However, the drawback is that they include some subjective  
205 steps. The temporal resolution of the IceMap SST is twice a week in the experiment period. Sea ice  
206 occurs most frequently in the Bay of Bothnia, with up to 100 ice covered days per year. However, sea  
207 ice can occur in all parts of the Baltic Sea and Danish straits, demonstrating the need for careful treat-  
208 ment of sea ice in the SST analysis.

209

### 210 **3.2 In situ data**

211 The observations from the German Maritime and Hydrographic Agency (BSH) moored buoy  
212 stations were collected as independent dataset to validate the assimilation results. The observations  
213 have high temporal resolution and long continuous record. The second dataset was downloaded from  
214 the Swedish Oceanographic Data Centre -SHARK database (<http://sharkweb.smhi.se>). SHARK mainly

215 contains low-resolution CTD data from a list of predefined standard stations in the Baltic Sea, as well  
216 as in Kattegat and Skagerrak. Only observations that have passed gross quality control procedures are  
217 collected into the SHARK database. This procedure includes, for example, location checks and local  
218 stability checks. In addition, validating data records from tide gauges are also used. The sea level  
219 anomaly measurements from tide gauges (sea level stations) are measured in a local height system and  
220 values are presented relative to theoretical mean sea level, a level calculated from many years of annu-  
221 al means, which takes into account the effect of land uplift and sea level rise. The values are averaged  
222 over one hour period.

223 Not all the available observations from satellite, moored buoys, CTDs, tide gauges were included  
224 in this study. To obtain the high assimilation quality results, another quality control was applied for  
225 these data before they were used into assimilation and validation. These controls include examination  
226 of forecast observation differences by excluding those observations for which the difference between  
227 the forecast and the measurement exceeded given standard maximum deviations. The criteria were set  
228 up empirically based on past validation results of the model (Liu et al. 2013). Furthermore, stations  
229 located on land, according to the NEMO-Nordic grid, were excluded. We also removed the duplicate  
230 records of these data.

231 The accuracy of observation error is difficult to be defined for all water points. ~~The observation~~  
232 ~~error mainly comes from the observation instrument itself, the observation representativeness, the~~  
233 ~~temporary reading error and imperfect retrieval algorithm.~~ The observation is commonly assumed to  
234 be spatially irrelevant, which results in an error covariance matrix that is time-invariant diagonal and  
235 its diagonal elements equal the variance of observation error. In this study, the observation error was  
236 estimated to one value as the sum of all observation uncertainties used in the analysis. Besides, the  
237 uncertainties of satellite SST varies from coast to the open sea, i.e. higher uncertainties in the coast  
238 region relative to the open sea. We used a constant standard deviation value of 0.4°C based on the  
239 standard deviation of satellite SST, which ranged from the ~0.1°C to ~0.5°C in the Baltic Sea (She et  
240 al. 2007, Høyer et al. 2016).

241

#### 242 **4. Configuration of LSEIK in the experiment**

243 As above mentioned, the initialization of the filter requires an initial analyzed state and a low  
 244 rank approximation of the corresponding estimation of error covariance matrix. The data assimilation  
 245 process was initialized by a free model simulation. First the model was spinning up 20 years to reach a  
 246 statistically steady state. Then a further (free-run) integration covered the period 2006-2009 was car-  
 247 ried out to generate a historical sequence of model state. To reduce the calculation cost, we took a  
 248 snapshot in every 6 days and saved 183 state vectors, [which includes sea level, temperature and salini-](#)  
 249 [ty, in](#) total to describe the model variability because successive states are quite similar. The initial en-  
 250 semble provided an estimate of the initial model state and its uncertainty before the assimilation of  
 251 SST observations. The quantity of the model variability was expected to be reasonably comparable  
 252 with the forecast error, which was dominated by misplacement of mesoscale features and varies in  
 253 location and intensity seasonally. Further, the very high frequencies of model variability were also  
 254 unfavourable in an ensemble of state vectors for SST data assimilation (Oke et al., 2005). Therefore, a  
 255 band-pass filter was used to remove the unwanted frequency of model variability. [To initial low rank](#)  
 256 [error covariance matrix, a](#) multivariable Empirical Orthogonal Functions (EOF) analysis was applied  
 257 [on the 183 state vectors of model variables \(sea level, temperature and salinity\). In the North Sea and](#)  
 258 [Baltic Sea, error covariances of different variables are not](#) uniform [and strongly dependent on whether](#)  
 259 [the variable resides in the open sea or coastal zone.](#) Each state variable was then normalized by the  
 260 inverse of its spatially averaged variance at every model [level](#). At last, 34 leading EOF modes were  
 261 kept and they explained 85% overall variability. Then the initial error covariance matrix was estimated  
 262 by  $P^a(t_0) \approx L_0 U_0 L_0^T$ , where the  $L_0$  is composited by the leading EOF modes and  $U_0$  is diagonal  
 263 matrix with the corresponding eigenvalues on its diagonal. [We used a time-invariant sample ensemble](#)  
 264 [to approximate the background error covariance during the experimental period \(Korres et al, 2004;](#)  
 265 [Liu et al. 2017\). This stationary ensemble affords a good approximation of the ocean's background](#)  
 266 [error covariance. Meanwhile, it is computationally efficient for our objective.](#)

267 A forgetting factor  $\rho$  was introduced to parameterize the imperfect model by amplifying the al-  
 268 ready existing modes of the background error (Nerger et al, 2006). The matrix  $U_i$  was calculated by

$$269 \mathbf{U}_i^{-1} = \rho(r + 1) \mathbf{T}^T \mathbf{T} + \mathbf{L}_i^T \mathbf{H}_i^T \mathbf{R}_i^{-1} \mathbf{H}_i \mathbf{L}_i \quad (8).$$

270 The localization scale is another important factor to the assimilation system, especially at the coastal  
271 region. Large correlation scale may transfer artificial increments to the positions far away from the  
272 analysis observation during the DA process. However, small correlation scale is prone to cause the  
273 singularity of ocean state around analyzed observation and break the continuity of the ocean state.  
274 Hence, an unreasonable scale causes the instability of the model integration or degrades the assimila-  
275 tion quality. Unfortunately, the accuracy length for the correlation is unknown for the North Sea and  
276 Baltic Sea. [The correlation length scale is to some extent dependent on the Rossby radius of defor-](#)  
277 [mation \(Losa et al., 2012\), which varies from ~ 200 km in the barotropic mode to ~ 10 km or even less](#)  
278 [in the baroclinic mode \(Fennel et al., 1991; Alenius et al, 2003\).](#) According to the former researches  
279 like Liu et al. (2013, 2017), a length scale of 70 km was specified for both the North Sea and Baltic  
280 Sea in this study. Not that this value may be not perfect and more accurate correlation length needs to  
281 be tested for LSEIK. For example, spatially variable length scales are the next step for the regional DA  
282 simulations.

283 [To define the forgetting factor, a one-month simulation experiment with varying the factor  \$\rho\$  was](#)  
284 [done in January 2010. At last, a factor  \$\rho = 0.3\$  resulted in the best assimilation performance. Further,](#)  
285 [we define a two-day assimilation window in assimilation experiment. As a result, the observations in](#)  
286 [the two days before the assimilation time were used to calculate the innovation with observation oper-](#)  
287 [ator. When we calculated the innovation we also changed the observation error according to the obser-](#)  
288 [vation time by](#)

$$\varepsilon = 0.4 \times \exp(-0.15\Delta t) \quad (9),$$

290 [here  \$\Delta t\$  is the absolute time difference between observation time and DA time.](#)

291

292

293

## 294 5. Results

295 In the following sub-sections, we conducted two runs with and without assimilation of the  
296 SST observations from the OSISAF database, both runs with the above setup of the analysis system.

297 Accordingly, the runs with and without assimilation are called ASSIM and FREE, respectively. We  
298 considered the evolution of SST based on 48-hourly local analysis from 1 January 2010 to 31 Decem-  
299 ber 2010. The [48-hourly forecast SST from](#) two runs was assessed with [observations from different](#)  
300 [dataset](#). Then we analyzed the impact of the data assimilation on the profile simulation of T/S. At last,  
301 we evaluated the system performance with respect to sea surface [anomaly](#) and sea ice, respectively.  
302

### 303 **5.1 Comparison with satellite data**

304 First, we presented [two cases to show the ocean state before and after](#) the assimilation of the  
305 OSISAF SST data in Fig. 2. The first case was given at 11 January 2010, a date with clear weather and  
306 many observations available. The model has obvious difficulties in reproducing the observed SST.  
307 The cold biases in the forecast were found in the Skagerrak, west coast of the Baltic proper and the  
308 Bothnian Bay, respectively. However, the warm biases appeared in the interior of the Baltic Sea and  
309 the Kattegat. The largest deviation in the FREE reached 2.2 °C at the Skagerrak. Apparently, tempera-  
310 ture by assimilation analysis agreed with the satellite-derived data much better. This correction at the  
311 analysis step has allowed us to reduce the deviation of the SST forecast from the observations. ~~The~~  
312 ~~SST bias of model forecast possibility has seasonal variability because of the errors in the forcing~~  
313 ~~and/or heat flux parameterization used in the ocean model (Fu et al. 2012).~~ [The](#) DA system simulation  
314 was also verified [at 2 June 2010](#), which has also many available OSISAF observations. The biases on  
315 2 June 2010 were obviously different from that on 11 January 2010. Moreover, it was found they had a  
316 roughly opposite bias signal. For example, relative to the OSISAF SST at the Baltic proper, Bothnian  
317 Sea and Bothnian Bay, FREE produced relatively warmer water [at January 11](#) and colder water [at 2](#)  
318 [June](#) (Fig. 2), respectively. After data assimilation, the analysis increments were appropriately added  
319 to the model field. In general, the SST DA has improved the [simulated SST](#) in both [cases](#) (Fig. 2).

320 Maps of annual averaged RMSE of SST from two runs relative to the IceMap observation are  
321 shown in Fig. 3. Obviously, the RMSE in FREE and ASSIM had different distribution in the Baltic  
322 Sea. In general, FREE had smaller error in the Skagerrak, eastern the Kattegat and the interior of the  
323 Bothnian Sea relative to other subbasin of the Baltic Sea. The largest RMSE was found at the connec-  
324 tion region between the Baltic proper and the Bothnian Sea. This could be caused by the shallow wa-

325 ter, complicated bathymetry and large observation biases in this area. It was also noted that the RMSE  
326 was larger in the coast region compared to its interior in the Baltic proper and Bothnian Sea. After the  
327 assimilation, the SST has been significantly improved. The RMSE of SST from ASSIM was generally  
328 smaller than 1.0 °C. However, there were still some regions where the improvements were relatively  
329 small and the RMSE of SST was greater than 1.0 °C. These large errors were predominantly located at  
330 the edge of the Baltic Sea and the Danish straits. For instance, the RMSE of SST was greater than 1.2  
331 °C at both the entrance of the Gulf of Finland and the west coast of the Bothnian Sea. The relatively  
332 small improvements were regularly caused by the rare observations or the less accurate observations  
333 near the coast water.

334 | \_\_\_\_\_ The overall daily averaged SST errors against the IceMap observations have been estimated  
335 (Fig. 4). The observations had better coverage in summer and autumn than in winter and spring. The  
336 variability of the number of observation directly affected the assessment of DA results. The model  
337 biases had pronounced seasonal variability, which had small values in spring and winter. In general,  
338 the assimilation provided better SST estimations. The free run had a RMSE of 1.47 °C. After the as-  
339 similation, the RMSE was reduced to 1.03 °C, whereas the bias was reduced by 0.73 °C. An interesting  
340 feature was that the SST error reduction due to the assimilation was almost consistent with the varia-  
341 bility of the number of IceMap observations. For example, the improvement became large with in-  
342 creasing the number of IceMap observations from March to June 2010. However, the number of ob-  
343 servations was kept constant during the period June-November 2010 and the improvement shown in  
344 both the bias and RMSE of SST did not exhibit large variability, which meant reliable performance of  
345 the DA system.

346

## 347 **5.2 Comparison with independent in-situ data**

348 The time series of T/S were compared with independent observations located at Arkona station  
349 (13.87°E, 54.88°N) in the Arkona Basin and at BY15 (20.05 °E, 57.33 °N) in the Eastern Gotland Ba-  
350 sin, respectively. These two stations were selected to verify the experiment results because of their  
351 | relatively completed observation records for the experiment period. In the Arkona Basin, the water  
352 depth was shallow and the water column can be well mixed between surface and bottom water. Thus,

353 the bottom T/S was largely affected by the surface dynamic (Liu et al. 2014). Relative to observations,  
354 the model had warm biases at this station (Fig. 5). ~~The temperatures differ by about 15–22 °C between~~  
355 ~~summer and winter.~~ At a depth of 25m, the observed temperature showed the largest variability, which  
356 was a good representation of the bottom characteristics of the mixed layer. In mid-August, the temper-  
357 ature was abruptly increased by 10°C at a depth of 25m and slightly decreased at surface, respectively.  
358 The reason is that the surface water suddenly sinks to deeper layers, which warm the deep water.  
359 However, this dynamic process hasn't reached to Arkona bottom and it didn't cause the obvious bot-  
360 tom temperature variability (Fig. 9). Both FREE and ASSIM had reproduced this process, whereas  
361 FREE showed larger temperature biases. To the salinity at the Arkona station, the surface observations  
362 were missing, the comparison at 7 m depth verified the subsurface simulations. The observations  
363 showed larger salinity variability in winter relative to summer. This pronounced seasonal variation is  
364 associated with the variation of fresh river runoff and net E–P (Evaporation–Precipitation) flux (Fu et  
365 al, 2012). At a depth of 7 m, salinity was obviously underestimated from April to September and over-  
366 estimated after November although the ASSIM had slightly better results compared to FREE. The DA  
367 also provided better simulation of salinity at 25 m depth. For example, the salinity bias in the October  
368 was reduced by 3 psu by DA. At a depth of 40 m, the saltwater inflows were observed, resulting in  
369 sudden increases of salinity. For instance, the salinity was increased by 3.5 psu in February followed  
370 by a decreasing trend. The variations were reproduced in both FREE and ASSIM, whereas the intensi-  
371 ty of the decreased process is weakly simulated with a difference of 3 psu and the inflow in March was  
372 not strong enough relative to the observed one. Observations also showed a large salinity variability  
373 amounts to 4–8 psu in the autumn. Although FREE and ASSIM had shown these changes, their mag-  
374 nitude was obvious weaker than observations. The possible reason was that the model's resolution was  
375 inadequate to well resolve the topography and eddies in this area. Both the large runoff and the com-  
376 plicated bathymetry posed challenges for the model to tackle the small-scale dynamic process in such  
377 a shallow basin. A higher resolution model perhaps was more preferable to study this dynamic pro-  
378 cess.

379 The Eastern Gotland Basin has deeper water depth compared to the Arkona Basin, in which the  
380 water column is permanently stratified and the halocline lies at about 60–80 m (Fu et al, 2012). The

381 mixing and sinking of T/S are hindered by the strong stratification. Unlike observations in the Arkona  
382 Basin (Fig. 5), the CTD observations at BY15 had lower temporal resolution with almost one observa-  
383 tion per month. In the mixing layer, it can be seen model had overestimated the temperature (Fig. 6).  
384 At a depth of 10 m, ASSIM has remarkably improved the simulation of temperature relative to FREE.  
385 The bias has been reduced by 3°C in the spring of 2010. At 175 m depth, observed temperature  
386 showed very small variation. The reason was that the main source for deep water ventilation is the  
387 saltwater inflows which are suppressed by runoff within a depth range of 75–135 m in the Eastern  
388 Gotland Basin (Vali et al. 2013). As a result, updating the bottom water is very slow. Both FREE and  
389 ASSIM overestimated the temperature in the spring and the beginning of summer of 2010. Further,  
390 ASSIM has increased the temperature bias after mid-summer relative to FREE. This result might be  
391 explained by that the strong correlation isn't expected between surface and layers below the halocline  
392 because of the strong stratification in this basin, which perhaps yield the artificial correction. There-  
393 fore, the improvement of the surface temperature cannot guarantee its positive influence on the bottom  
394 temperature. To the salinity, the model had less accurate simulation with generally low salinity biases  
395 at 10 m depth. ASSIM provided better salinity simulation compared to FREE. At 70 m depth, the  
396 small variation of salinity was found after DA. Moreover, at 175 m depth, the observation had very  
397 small variability about 0.1 psu. In general, both experiments have reproduced these variations. How-  
398 ever, FREE increased salinity by 0.2 psu from March to April relative to the observation, which  
399 caused the overall salinity overestimated amount to 0.2 psu. This increasing process wasn't shown in  
400 observations and the reason remained unclear. The DA has shown slight improvement, but it still salt-  
401 er than the observations.

402 The mixed layer depth (MLD) was calculated at the Arkona and BY15 station and compared with  
403 the SHARK observation in Fig. 7. We used the temperature criterion to define the MLD, i.e., the depth  
404 at which the temperature deviated from the surface value by 0.5 °C (Fu et al., 2012). Figure 7 shows  
405 that the MLD at Arkona had larger variability relative to the MLD at BY15. The reason contributed to  
406 this feature is that the deeper water at Arkona is easy affected by wind forcing because of the shallow  
407 bathymetry and well mixing, whereas the temperature variation in upper water at BY15 difficulty in-  
408 fluences the deeper water because of the strong stratification. Both runs had reproduced the MLD var-

409 iability feature similar as the observations. For example, the minimum MLD appeared in summer,  
410 which was about several meters. The assimilation of satellite SST caused strong changes in the MLD  
411 at both stations, especially in winter. One explanation was that the Baltic Sea was largely affected by  
412 wind forcing and the winter wind was much stronger than the summer wind. Further, strong heating in  
413 summer promoted stratification in summer and shoaled the MLD.

414 Further, the temporal and spatial distribution of the SHARK observations is shown in Fig.8.  
415 These observations were unevenly distributed in the Baltic Sea. In the Skagerrak, the observations  
416 appeared at the Danish and Swedish coast. However, in the Bornholm Basin, Kattegat, and Baltic  
417 proper, the observations mainly were found in the central and the Swedish coast side. There were also  
418 many observations in the Bothnian Sea and rare observations in the central of the Bothnian Bay. It  
419 must be noticed that there aren't SHARK observations in both the Gulf of Finland and Gulf of Riga  
420 during the experiment period. Moreover, these SHARK profiles in the first four months were mainly  
421 located from the Skagerrak to the Baltic proper, which are relatively rare in the northern Baltic Sea. In  
422 the Bothnian Bay, the observations are mainly in the winter period.

423 Figure 9 shows the change of overall bias and RMSE of T/S with depth against the SHARK  
424 dataset. In the Baltic Sea, DA had large impact on the temperature forecast in the water above 100 m.  
425 The RMSE showed that the forecast of temperature was obviously improved from surface to thermo-  
426 cline in the ASSIM and the improvements generally decreased with depth. Above 100 m, the overall  
427 RMSE of temperature in ASSIM was decreased by 21.38% (from 1.59 to 1.25 °C). It was also found  
428 the temperature error had similar variability as the warm biases in two runs. In the transition zone, the  
429 RMSE in the ASSIM was reduced by 5.59% and -20.31% above and below 100 m relative to the  
430 FREE, respectively. Below 90 m, the temperature was also over-adjusted, which changed the warm  
431 bias to cold bias. It is worth noting that the number of the deeper water observation in the transition  
432 zone is substantially less than that in the Baltic Sea. For the salinity, both RMSE and bias of the AS-  
433 SIM showed very minor changes relative to the FREE inside the Baltic Sea. For the water above 100  
434 m, the total RMSE of salinity was increased by 3.48% (from 1.15 psu in the FREE to 1.19 psu in the  
435 ASSIM) in the transition zone and 1.04% (from 0.96 psu in the FREE to 0.97 psu in the ASSIM) in  
436 the Baltic Sea.

437

### 438 5.3 Sea Level Anomaly

439 SLA represents a vertically integrated effect of the T/S variations over the whole water col-  
440 umn. The accurate simulation of SLA is thus a good indicator of the model performance. Therefore,  
441 validating the impact of SST assimilation on the simulation of SLA is very important to the Baltic Sea  
442 forecast. The observations from the 24 tide gauge stations were used. These gauge stations are mainly  
443 located at the Swedish coast ([see Fig.8b](#)). Since only the SST is assimilated in this study, the SLA  
444 observations are completely independent.

445 [We calculated the RMSE and correlation coefficients for both the FREE and ASSIM against the](#)  
446 [observations from tide gauges \(Fig. 10\). The overall RMSE was reduced by 1.8% and the correlation](#)  
447 [coefficients were slightly increased. Among these stations, RMSE at the Oskarshamn was decreased](#)  
448 [by 5.6%, which is larger than that in other station. The minimum RMSE change of SLA was seen at](#)  
449 [the Klagshamn. For the correlation coefficient, improvement on the SLA by the DA is very small.](#)  
450 [Simrishamn station showed the biggest change of correlation coefficient, which is 1.1%. The RMSE](#)  
451 [and correlation comparison demonstrated that the SST DA has generally positive effects on the fore-](#)  
452 [cast of the SLA.](#)

453 [In addition, the time series of the SLA error discrepancy \(ASSIM minus FREE\) in two runs at](#)  
454 [four stations were selected to evaluate the simulation results \(Fig. 11\). These four stations were select-](#)  
455 [ed to represent the model performance at different positions of the Swedish coast. Two runs showed](#)  
456 [evidently different performance in these four stations. The variability of the SLA difference between](#)  
457 [two experiments at the Smogen station had higher frequency compared to other stations. The reason](#)  
458 [was that the Smogen station was located at the transition zone where the water had higher frequency](#)  
459 [variations caused by the brackish Baltic in/outflowing relative to other three stations. At these four](#)  
460 [stations, the improvements were mainly in later spring and summer, whilst the degraded simulations](#)  
461 [were mostly happened after Mid-September, respectively.](#) The SST assimilation had less impact in late  
462 winter and early spring compared to other seasons. Besides, the impact of SST assimilation on SLA  
463 simulation was not same in the four positions. For instance, [during the period from Mid-November to](#)  
464 [Mid-December, the SLA in ASSIM was improved at Simrishamn and degraded at both Ratan and](#)

465 [LandsortNorra stations, respectively](#). This phenomenon was possibly caused by the imperfect correla-  
466 tion between SST and SLA in the stationary samples. Further, these steric small changes of SLA by  
467 [DA](#) were what we expected because only SST was assimilated into Nemo-Nordic.

468

#### 469 **5.4 Sea ice**

470 Sea ice in the Baltic Sea occurs primarily in its north region and influences the Baltic climate.  
471 Accurate detecting the sea ice is very useful to the northern Baltic living because too much or too little  
472 sea ice can be a problem for wildlife and people. Sea ice concentration (SIC) [and Sea ice extent \(SIE\)](#)  
473 [are two](#) important and common indicator to modeling sea ice environment. We assessed the SIC [and](#)  
474 [SIE](#) from simulations against the IceMap observations in Fig. [12-13](#). Differ from the daily evaluation  
475 in Losa et al. (2014), the monthly mean SIC was used to represent the general status of sea ice in the  
476 Baltic Sea. Besides, SIC in January, February and December showed the variation of the sea ice in  
477 winter.

478 In January 2010, the observations showed large ice coverage in the Bothnian Bay and the Gulf  
479 of Finland and small SIC in the Gulf of Riga, respectively. Model generally reproduced this distribu-  
480 tion of sea ice. However, FREE simulated too much sea ice in the Gulf of Finland and the eastern  
481 coast of the Baltic proper relative to observations. For example, SIC from FREE almost to 30% higher  
482 than observations along the Estonia coastline. It could be seen that the SST DA reduced these biases.  
483 The reason is the SST DA modified the thermal expansion by providing the well temperature fields  
484 above the thermocline. The temperature in February became colder relative to January in the Baltic  
485 Sea. As a result, the sea ice in February extended to the Bothnian Sea and the whole Gulf of Riga.  
486 Observation also showed small SIC in Kattegat and Skagerrak. Model simulated higher SIC in the  
487 Bothnian Sea with largest biases along the Swedish and Finnish coast. As an example, the observed  
488 ice in the Bothnian Sea was characterized by concentrations mainly smaller than 0.5, whereas modeled  
489 ice in FREE had concentration greater than 0.9 in the shallow region of the Bothnian Sea. FREE also  
490 had smaller ice coverage with lower SIC in the transition zone between the North Sea and the Baltic  
491 Sea relative to IceMap. After the SST assimilation, ASSIM reduced SIC in the Bothnian Bay and the  
492 west coast of the Baltic Sea, which was closer to the observations. The ice in ASSIM didn't have ob-

493 various variation in Kattegat and Skagerrak yet. ASSIM also reduced too much ice at the southern of the  
494 Bothnorn Basin. The reason is that the satellite SST observations had limited accuracy near the coast  
495 and they could bring artificial information into the modeling. In March, compared to observation, the  
496 FREE produced low SIC in the western coast of the Bothnian Sea, Gulf of Finland, Gulf of Riga and  
497 the connect zone between the Bothnian Sea and Gulf of Finland. However, the model SIC in the FREE  
498 was higher than IceMap in the interior the Bothnian Bay. For instance, the SIC from FREE in the  
499 western Bothnian Sea was 40% higher than observation. In the south coast of the Arkona basin and  
500 Baltic proper, the FREE failed to reproduce the sea ice as in observation. After the DA, the high SIC  
501 was decreased in western Bothnian Sea and closer to that in IceMap in Bothnian Sea. In the Gulf of  
502 Finland and Gulf of Riga, the SIC error was increased in the ASSIM. In April, the large SIC error in  
503 the FREE was shown in the Bothnian Sea, the Bothnian Bay, Gulf of Riga and Gulf of Finland, where  
504 no clear improvements were seen in the ASSIM. In December, sea ice coverage was smaller because  
505 of relatively warm temperature compared to that in other winter month. Most of the sea ice with high  
506 concentration was observed at the edge of the Bothnian bay. Nevertheless, high concentration ice in  
507 FREE also happened at the transition zone between the Bothnian Sea and Bothnian bay. Relatively,  
508 ASSIM reduced the high concentration biases of sea ice. By contrast, both ASSIM and FREE had  
509 lower concentration ice than observation in the eastern coast of the Bothnian Sea. The SIC from AS-  
510 SIM was relatively lower than that from FREE in the northern Finish coast, whereas the observations  
511 had high concentration ice there.

512 The daily SIE from FREE and ASSIM was compared with observations in Fig.13. The observed  
513 SIE was generally increased from January to February and reached the maximum in mid-February.  
514 During the period of March-May, SIE was decreased as temperature was increasing. SIEs in both the  
515 FREE and ASSIM experiments were generally underestimated by comparison with the observation in  
516 2010, especially in the period from Mid-March to early April. The SIE bias in both runs was roughly  
517 increased from January to early April. In early April, the maximum negative bias of SIE was found to  
518 be 105000 km<sup>2</sup> for ASSIM and 10000 km<sup>2</sup> for FREE. The impact of SST assimilation on the SIE was  
519 positive during the phase of sea ice formation. For example, the SIE bias was reduced 25000 km<sup>2</sup> at  
520 end of February and in the Mid-December. However, during the phase of sea ice melting (March to

521 [April](#)), the SIE error was increased in ASSIM even with the error of SST decreased. For example, the  
522 [SIE bias in ASSIM was increased by 42000 km<sup>2</sup> relative to FREE in the early March. These increased](#)  
523 [SIE error in March mainly happened in the Gulf of Riga and Gulf of Finland \(Fig.11\).](#)

524

## 525 **6. Conclusion and discussions**

526 A DA system based on a [LSEIK](#) filter has been coupled to the NEMO circulation model of the  
527 North and Baltic Seas. The method was successfully applied for assimilating high resolution satellite  
528 SST data. We demonstrated that, over the period of 2010, the agreement of the SST forecast with the  
529 independent satellite observation was improved by ~ 29.93% in comparison with the regular forecast  
530 without DA. The assimilation quality is directly related to the number of observation.

531 Compared with independent in-situ data from SHARK, the RMSE [of temperature](#) was reduced  
532 by [21.38% and 5.59% for the water above 100 m inside and outside of the Baltic Sea, respectively.](#)  
533 However, in the deeper layers, the temperature was slightly degraded [in the Baltic Sea](#). This is partial-  
534 ly caused by the artificial correlation between surface layer and deeper layers. The improvement of  
535 temperature by SST DA can't guarantee corresponding improvement of the salinity. [The statistics](#)  
536 [displays the salinity RMSE was increased by 1.04% and 3.48% in the transition zone and the Baltic](#)  
537 [Sea, respectively.](#) Both ASSIM and FREE have captured the main dynamic process in the Baltic Sea,  
538 for example, the inflow and the sink. However, ASSIM is closer to the observed one relative to  
539 FREE.

540 [The forecast results were further validated with](#) the independent SLA observations. [The result](#)  
541 shows that all RMSEs and correlations for all 21 stations are smaller than 0.12 m and greater than  
542 0.86, respectively. After DA, the SLAs at these stations have been slightly improved. In general, the  
543 RMSE [was reduced by 1.8%](#) and correlation coefficients were [slightly](#) increased, respectively. Fur-  
544 ther, the model-observation comparison at selected four stations indicates that these improvements are  
545 mainly in later of spring and summer. The comparisons also denote the SST assimilation has less im-  
546 pact in the late winter and early spring relative to other seasons.

547 When compared with monthly mean observations of SIC, both assimilation run and free run

548 reproduced main [spatial](#) distributions of sea ice in the Baltic Sea. [During the sea ice formation period,](#)  
549 [the SST assimilation has improved the results of SIC from\\_FREE in the Gulf of Finland, the Bothnian](#)  
550 [Sea and eastern coast of the Baltic proper. However, minor improvements were found in Kattegat and](#)  
551 [Skagerrak. Besides, over the sea ice melting period, the SIE comparison showed the SST assimilation](#)  
552 [increased the SIE error, especially in the Gulf of Finland and Gulf of Riga.](#)

553 [The daily MLD from two runs has been compared with the observations at Arkona and BY15](#)  
554 [stations. Model could capture the variability features of the MLD. Similar as Fu et al.\(2012\), it was](#)  
555 [found that SST assimilation had less impact on the MLD in summer than that in winter. In general, the](#)  
556 [SST DA produced less influences on the MLD in the deeper region \(BY15\) relative to that in the shal-](#)  
557 [low region \(Arkona\).](#)

558 [Further, the reliability of the DA system is worth being assessed. In Rodwell et al.\(2006\), a per-](#)  
559 [fect reliable system error variance for ensemble assimilation was calculated by the sum of the variance](#)  
560 [of the sample ensemble, the square of innovation\(misfit between observation and model\) and the vari-](#)  
561 [ance of observation at assimilation time. In this study, we used a constant observation error similar to](#)  
562 [Rodwell et al. \(2016\) because our DA design is different from that paper. The major difference be-](#)  
563 [tween these two studies is that we estimate the background error covariance from stationary ensemble](#)  
564 [and avoid the perturbation of observation error. Therefore, the variance of the sample ensemble and](#)  
565 [observation is univariate and the diagnostic of the assimilation stability can be directly obtained from](#)  
566 [the forecast error like the RMSE in Fig.4.](#)

567 The results of the SST assimilation are encouraging and the assimilation helps to ameliorate  
568 some model deficiencies such as the simulation of sea ice in the Gulf of Finland. However, some prob-  
569 lems need to be further addressed in the SST DA in the future: firstly, the SST assimilation has worse  
570 influence on the simulation of salinity in the upper layers and temperature in the deeper layers. Losa et  
571 al.(2012) denoted that the salinity simulation quality crucially depends on the assumptions about the  
572 model and data error statistics. Here a stationary ensemble sample was used to represent the correla-  
573 tion between T/S and between surface and deep water. These relationships could be changed with the  
574 varying dynamics and forcing conditions. More sophisticated assumption should be used in the DA of  
575 Baltic Sea. Secondly, the SHARK observations in this study are absent at the Gulf of Finland and Gulf

576 of Riga. This denotes the validation results with SHARK observation didn't include the evaluation of  
577 the simulation of T/S in deep water of these two basins. Thirdly, the univariate localization scale used  
578 in this study could be another problem. The spreading of observation information strongly depended  
579 on the correlation scale ~~around the observation position~~. The large localization scale can introduce the  
580 artificial information, which could degrade the assimilation quality. A flow-dependent background  
581 error covariance with varying correlation scale may be more appropriate for the Baltic Sea with com-  
582 plex bathymetry and rich dynamics. Fourthly, the remote sensing observations near the coast could  
583 have large bias because of the limit of the instrument itself. More strict quality controlling method  
584 needed to be used for the satellite coastal observations before their assimilation.

585

## 586 **Acknowledgment**

587

588 The research presented in this study was funded by the Swedish Space Board within the project 'As-  
589 simulating SLA and SST in an operational ocean forecasting mode for the North Sea and Baltic Sea  
590 using satellite observations and different methodologies' (grant no.172/13).

591

## 592 **References**

593 Adcroft, A., and Campin, J. M.: Re-scaled height coordinates for accurate representation of free-  
594 surface flows in ocean circulation model, *Ocean Modell.*, 7, 269–284, 2004.

595

596 [Alenius, P. A., Nekrasov, A., and Myrberg, K.: Variability of the baroclinic Rossby radius in the Gulf  
597 of Finland, \*Cont. Shelf Res.\*, 23 \(6\), 563–573, 2003.](#)

598

599 Beckmann, A., and Döscher, R.: A method for improved representation of dense water spreading over  
600 topography in geopotential-coordinate models, *J. Phys. Oceanogr.*, 27, 581–591, 1997.

601

602 Brisson, A., Le Borgne, P., and Marsouin, A.: Results of one year of preoperational production of sea

603 surface temperatures from GOES-8, *J. Atmos. Oceanic Technol.*, 19(10), 1638–1652, 2002.

604

605 Dahlgren, P., Källberg, P., Landelius, T. and Undén, P.,: EURO4M Project Report, D 2.9 Comparison  
606 of the Regional Reanalyses Products with Newly Developed and Existing State-of-the Art Systems.  
607 Technical Report, Online at: <http://www.euro4m.eu/Deliverables.htm>, 2014.

608

609 [Donnelly, C., Andersson, J. C., and Arheimer, B.: Using flow signatures and catchment similarities to](#)  
610 [evaluate the E-HYPE multi-basin model across Europe, \*Hydrological Sciences Journal\*, 61, 255–273,](#)  
611 [2016.](#)

612

613 Egbert, G. D., and Erofeeva, S. Y.: Efficient inverse modeling of barotropic ocean tides, *J. Atmos.*  
614 *Oceanic Technol.*, 19(2), 183–204, doi: 10.1175/1520-0426, 2002.

615

616 [Fennel, W., Seifert, T., and Kayser, B.: Rossby radii and phase speeds in the Baltic Sea. \*Cont. Shelf\*](#)  
617 [Res., 11\(1\), 23–26, 1991.](#)

618

619 Fu, W.W., She, J., and Dobrynin, M.: A 20-year reanalysis experiment in the Baltic Sea using  
620 three-dimensional variational (3DVAR) method. *Ocean Sci.*, 8, 827–844, 2012.

621

622 Galperin, B., Kantha, L. H., Hassid, S., and Rosati A.: A quasi-equilibrium turbulent energy model for  
623 geophysical flows, *J. Atmos. Sci.*, 45, 55–62, 1988.

624

625 Haines, K.: Ocean data assimilation. In: *Data Assimilation: Making Sense of Observations.* . Springer-  
626 Verlag, Berlin Heidelberg, pp. 517-548. ISBN 9783540747024, 2010.

627

628 Hordoir, R., Axell, L., Löptien, U., Dietze, H., and Kuznetsov, I.: Influence of sea level rise on the  
629 dynamics of salt inflows in the Baltic Sea, *J. Geophys. Res. Oceans*, 120, doi:10.1002/2014JC010642,  
630 2015.

631

632 Hordoir, R., Dieterich, C., Basu, C., Dietze, H., and Meier M.: Freshwater outflow of the Baltic Sea  
633 and transport in the Norwegian current: A statistical correlation analysis based on a numerical experi-  
634 ment, *Cont. Shelf Res.*, 64, 1–9, doi:10.1016/j.csr.2013.05.006, 2013.

635

636 Høyer J.L., and Karagali, I.: Sea Surface Temperature Climate Data Record for the North Sea and  
637 Baltic Sea. *JOURNAL OF CLIMATE*. 29, 2529–2541, 2016.

638

639 [Janjić, T., Nerger, L., Albertella, A., Schröter, J., Skachko, S., On domain localization in ensemble  
640 based Kalman filter algorithms. \*Monthly Weather Review\*, 136 \(7\), 2046–2060, 2011.](#)

641

642 Kilpatrick, K. A., Podesta, G. P., and Evans, R.: Overview of the NOAA/NASA Advanced Very High  
643 Resolution Radiometer Pathfinder algorithm for sea surface temperature and associated matchup data-  
644 base, *J. Geophys. Res.*, 106(C5), 9179–9197, doi:10.1029/1999JC000065, 2001.

645

646 Large, W. G., and Yeager, S.: Diurnal to decadal global forcing for ocean and sea-ice models: The  
647 data sets and flux climatologies, NCAR Tech. Note, NCAR/TN-4601STR, CGD Div. of the Natl.  
648 Cent. for Atmos. Res., 2004.

649

650 Leclair, M., and Madec, G.: A conservative leapfrog time stepping method, *Ocean Modell.*, 30, 88–94,  
651 doi:10.1016/j.ocemod.2009.06.006, 2009.

652

653 Leppäranta, M., and Myrberg, K.: *The Physical Oceanography of the Baltic Sea*, pp. 378, Springer-  
654 Verlag, Berlin-Heidelberg, New York, 2009.

655

656 Levitus, S., and Boyer, T. P.: Salinity, in *World Ocean Atlas 1994*, NOAA Atlas NESDIS, vol. 3, 99  
657 pp., U.S. Gov. Print. Off., Washington, D. C., 1994.

658

659 Liu, Y., Zhu, J., She, J., Zhuang, S. Y., Fu, W.W., and Gao, J.D.: Assimilating temperature and salini-  
660 ty profile observations using an anisotropic recursive filter in a coastal ocean model. *Ocean Model.* 30,  
661 75–87, 2009.

662

663 Liu, Y., Meier, H. E. M., and Axell, L.: Reanalyzing temperature and salinity on decadal time scales  
664 using the ensemble optimal interpolation data assimilation method and a 3-D ocean circulation model  
665 of the Baltic Sea. *J. Geophys. Res.Oceans.*, 118, 5536–5554, 2013.

666

667 Liu, Y., Meier, H. E. M., and Eilola, K.: Improving the multiannual, high-resolution modelling of bio-  
668 geochemical cycles in the Baltic Sea by using data assimilation, *Tellus A*, 66, 24908,  
669 doi:10.3402/tellusa.v66.24908, 2014.

670 Liu, Y., Meier, H. E. M., and Eilola, K.: Nutrient transports in the Baltic Sea – results from a 30-year  
671 physical–biogeochemical reanalysis. *Biogeosciences*, 14, 2113–2131, 2017.

672

673 Losa S.N., Danilov, S., Schröter, J., Nerger, L., Maßmann, S., and Janssen, F.: Assimilating NOAA  
674 SST data into the BSH operational circulation model for the North and Baltic Seas: Inference about  
675 the data. *Journal of Marine Systems*, 105–108,152–162, 2012.

676

677 Losa S.N., Danilov, S., Schröter, J., Janjic, J., Nerger, L., and Janssen, F.: Assimilating NOAA SST  
678 data into the BSH operational circulation model for the North and Baltic Seas: Part 2. Sensitivity of  
679 the forecast's skill to the prior model error statistics. *Journal of Marine Systems*, 259–270, 2014.

680

681 Madec, G.: NEMO ocean engine, version 3.3, Note du Pôle de modélisation de l’Inst. Pierre-Simon  
682 Laplace 27, Inst. Pierre-Simon Laplace, Paris. (Available at <http://www.nemo-ocean.eu/>), 2010.

683

684 Malanotte-Rizzoli, P, and Tziperman, E.: The oceanographic data assimilation problem: overview,  
685 motivation and purposes. In *Modern Approaches to Data Assimilation in Ocean Modeling*, Amster-  
686 dam: Elsevier, 3–17, 1996.

687

688 [Nerger, L., Danilov, S., Hiller, W., and Schröter, J.: Using sea level data to constrain a finite-element](#)  
689 [primitive-equation ocean model with a local SEIK filter. Ocean Dynamics 56, 634–649, 2006.](#)

690

691 Nowicki, A., Dzierzbicka-Głowacka, L., Janecki, M., and Kałas, M.: Assimilation of the satellite SST  
692 data in the 3D CEMBS model. *Oceanologia*, 57, 17–24, 2015.

693

694 O’Dea E. J., Arnold, A. K., Edwards, K. P., Furner, R., Hyder, P., Martin, M. J., Siddorn, J. R.,  
695 Storkey, D., While, J., Holt, J. T., and Liu H.: An operational ocean forecast system incorporating  
696 NEMO and SST data assimilation for the tidally driven European North-West shelf, *Journal of Opera-*  
697 *tional oceanography*, 5(1), 3-17, 2012.

698

699 Oke, P. R., Schiller, A., Griffin, D. A., and Brassington, G. B.: Ensemble data assimilation for an ed-  
700 dy-resolving ocean model of the Australian Region. *Q. J. Roy. Meteorol. Soc.* 131, 3301–3311, 2005.

701

702 [Omstedt, A., Elken, J., Lehmann, A., Leppäranta, M., Meier, H.E.M., Myrberg, K., and Rutgersson,](#)  
703 [A.: Progress in physical oceanography of the Baltic Sea during the 2003–2014 period. \*Progress in\*](#)  
704 [Oceanography, 128, 139-171, 2014.](#)

705

706 Pham, D.T.: Stochastic methods for sequential data assimilation in strongly nonlinear systems. *Mon.*  
707 *Weather Rev.* 129, 1194–1207, 2001.

708

709 [Rodwell, M. J., Lang, S. T. K., Ingleby, N. B., Bormann, N., Hólm, E., Rabier, F., Richard-](#)  
710 [son, D. S., and Yamaguchi, M.: Reliability in ensemble data assimilation, \*Q. J. Roy. Meteor. Soc.\*,](#)  
711 [142, 443–454, doi:10.1002/qj.2663, 2016.](#)

712

713 Samuelsson, P., Jones, C., Willen, U., Ullerstig, A., and co-authors.: The Rossby Centre Regional  
714 Climate model RCAS3: model description and performance, *TellusA*, 63, 4–23, 2011.

715  
716  
717  
718  
719  
720  
721  
722  
723  
724  
725  
726  
727  
728  
729  
730  
731  
732  
733  
734  
735  
736  
737  
738  
739  
740  
741  
742

She, J, Høyer, J. L., and Larsen, J.: Assessment of sea surface temperature observational networks in the Baltic Sea and North Sea. *Journal of Marine Systems* 65, 314–335, 2007.

Stramska, M., and Białogrodzka, J.: Spatial and temporal variability of sea surface temperature in the Baltic Sea based on 32-years (1982—2013) of satellite data. *Oceanologia*, 57, 223–235, 2015.

Tranchant B., Reffray, G., Greiner, E., Nugroho, D., Koch-Larrouy, A., and Gaspar, P.: Evaluation of an operational ocean model configuration at 1/12° spatial resolution for the Indonesian seas (NEMO2.3/INDO12) –Part 1: Ocean physics. *Geosci. Model Dev.*, 9, 1037–1064, 2016.

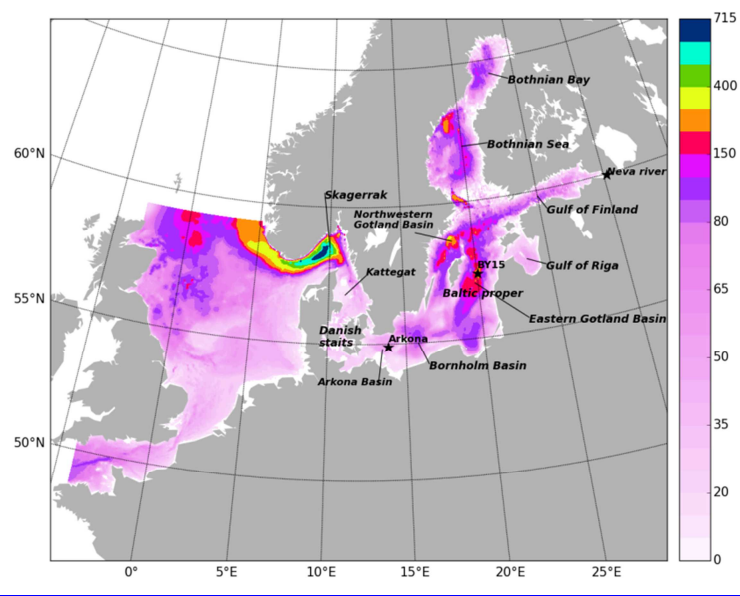
Umlauf, L., and Burchard, H.: A generic length-scale equation for geophysical turbulence models, *J. Mar. Syst.*, 61, 235–265, 2003.

Vancoppenolle, M., Fichefet, T., Goosse, H., Bouillon, S., Madec, G., and Maqueda, M. A. M.: Simulating the mass balance and salinity of arctic and Antarctic sea ice, *Ocean Modell.*, 27(1–2), 33–53, doi:10.1016/j.ocemod.2008.10.005, 2008.

Väli, G., Meier, H. E. M., and Elken, J.: Simulated halocline variability in the Baltic Sea and its impact on hypoxia during 1961–2007, *J. Geophys. Res.-Ocean.*, 118, 6982–7000, doi:10.1002/2013JC009192, 2013.

Walton, C. C., Pichel, W. G., Sapper, F. J., and May, D. A.: The development and operational application of nonlinear algorithms for the measurement of sea surface temperatures with NOAA polar-orbiting environmental satellites, *J. Geophys. Res.*, 103(C12), 27,999–28,012, doi:10.1029/98JC02370, 1998.

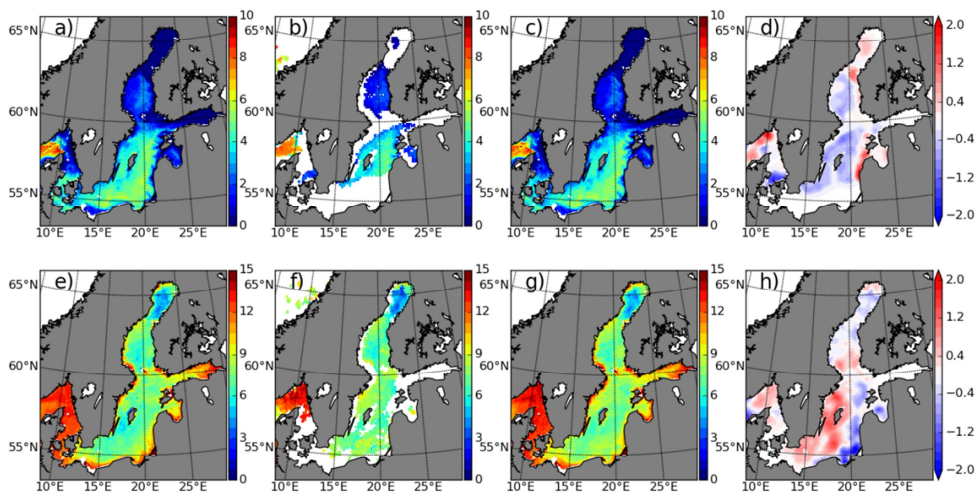
743  
744  
745  
746  
747  
748  
749  
750



751  
752  
753  
754  
755  
756  
757  
758  
759  
760  
761

Figure 1. Geographical domain and bathymetry (in m) of the NEMO-Nordic configuration.

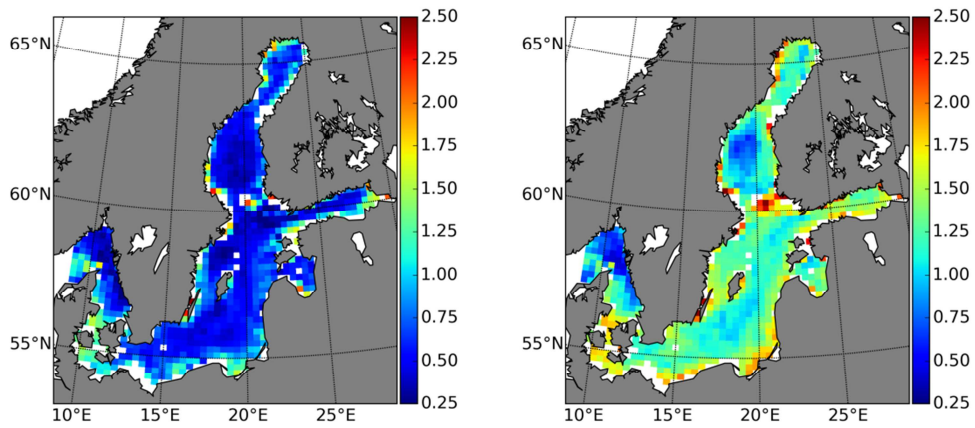
762  
763  
764  
765  
766  
767  
768



769  
770  
771  
772  
773  
774  
775  
776  
777  
778  
779  
780  
781

Figure 2. Map of SST from FREE (a,e), OSISAF (b, f), ASSIM (c, g) and the assimilation increments (d, h) on 11 January 2010 (first row) and 2 June 2010 (second row), respectively.

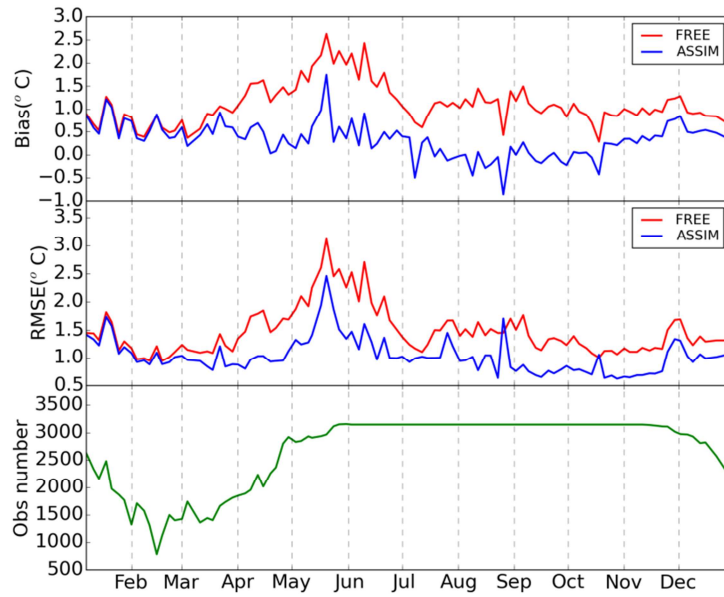
782  
783  
784  
785  
786



787  
788  
789  
790  
791  
792  
793  
794  
795  
796  
797  
798  
799  
800  
801  
802

Figure 3. Map of the RMSE of SST from ASSIM (left panel) and FREE (right panel) calculated against IceMap SST in 2010, respectively.

803  
804  
805  
806  
807

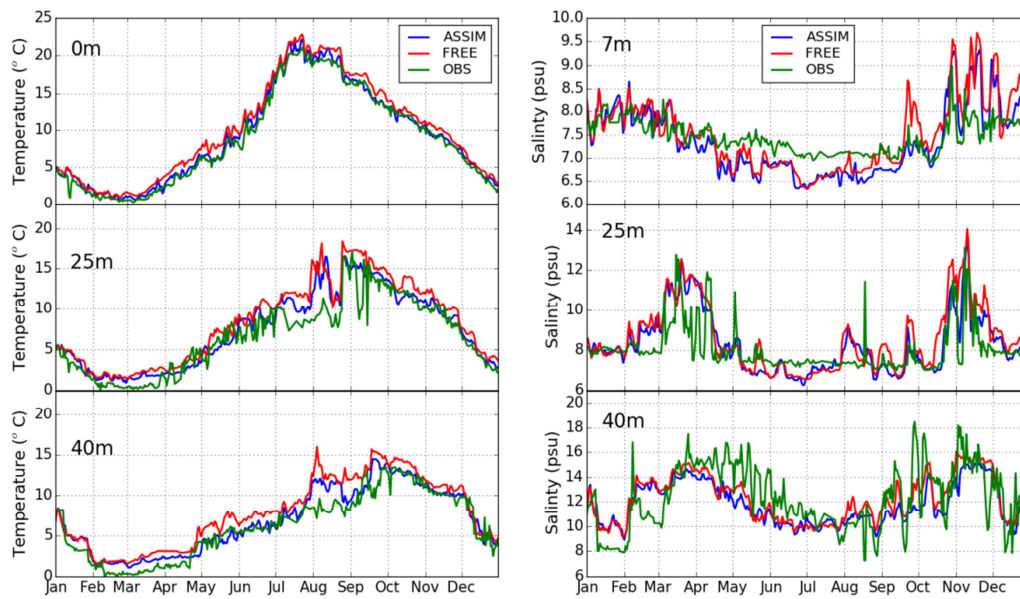


808  
809  
810  
811  
812  
813  
814  
815  
816  
817  
818  
819  
820  
821

Figure 4. The evolution of basin-averaged bias and RMSE of SST from FREE and ASSIM relative to IceMap SST and the number of IceMap observation in 2010.

822

823



824

825 Figure 5. The time series of temperature (left panel) at a depth of 0, 25 and 40 m and salinity (right  
826 panel) at a depth of 7, 25 and 40 m at the Arkona station (13.87°E, 54.88°N ), respectively.

827

828

829

830

831

832

833

834

835

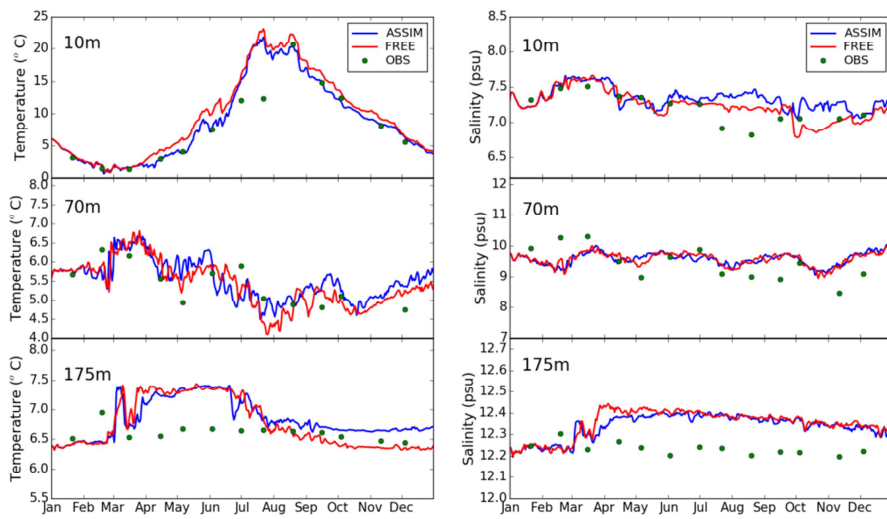
836

837

838

839

840



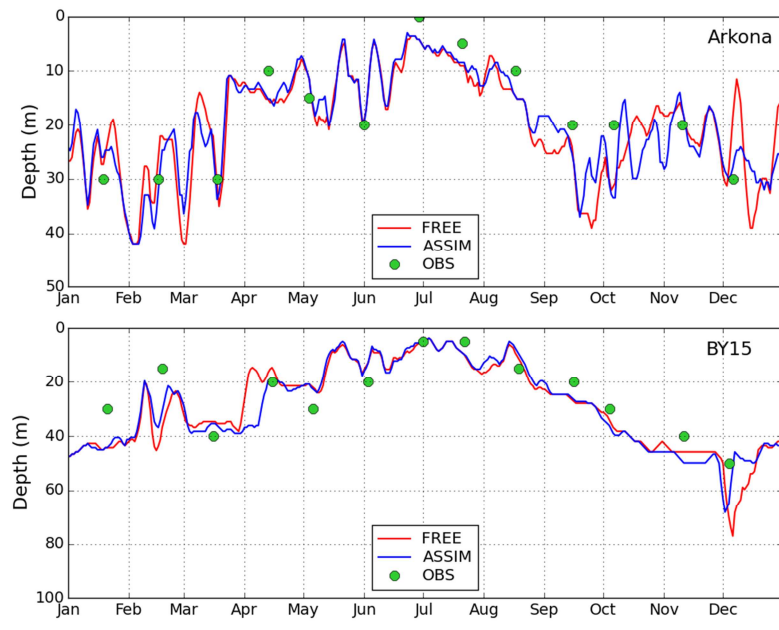
841

842 Figure 6. The time series of temperature (left panel) and salinity (right panel) at the BY15 station  
 843 (20.05°E, 57.33°N ) at a depth of 10, 70 and 175 m, respectively.

844

845

846



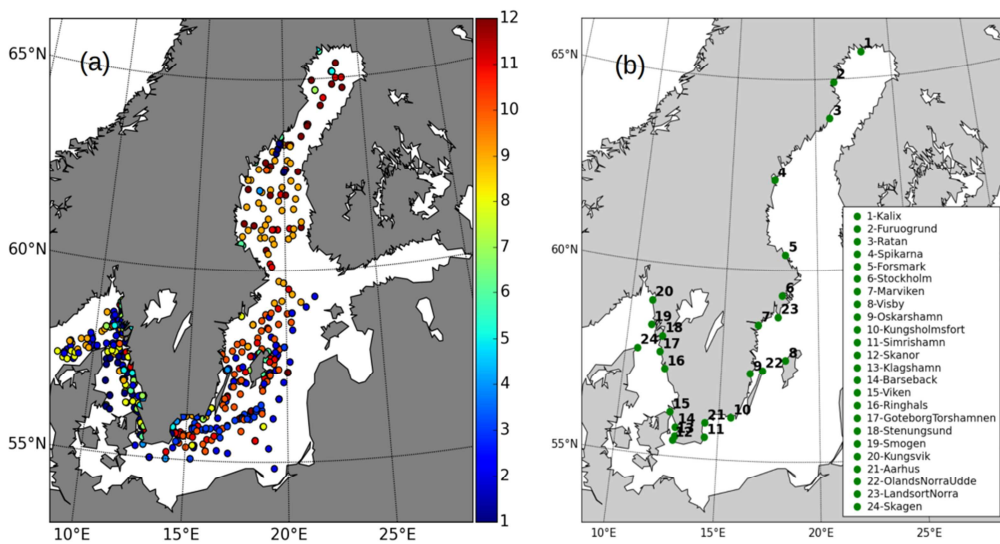
847

848 [Figure 7. The time series of mixed layer depth at Arkona and BY15 station.](#)

849

850

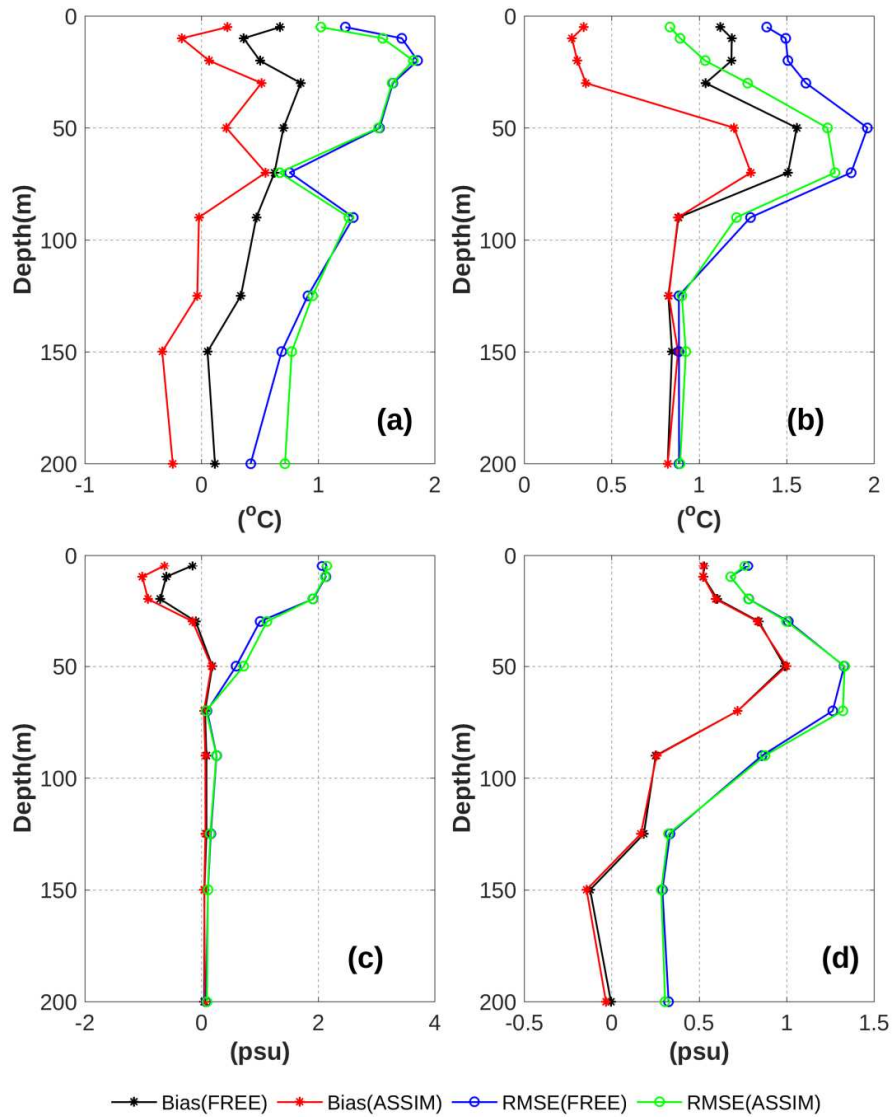
851  
852  
853  
854  
855  
856  
857  
858  
859  
860



861  
862  
863  
864  
865  
866  
867  
868  
869

Figure 8. (a) Map of the temperature and salinity profiles from SHARK database in 2010. The colors show the observations months. (b) The tide gauges station along the Swedish coast.

870  
871  
872  
873  
874  
875



876

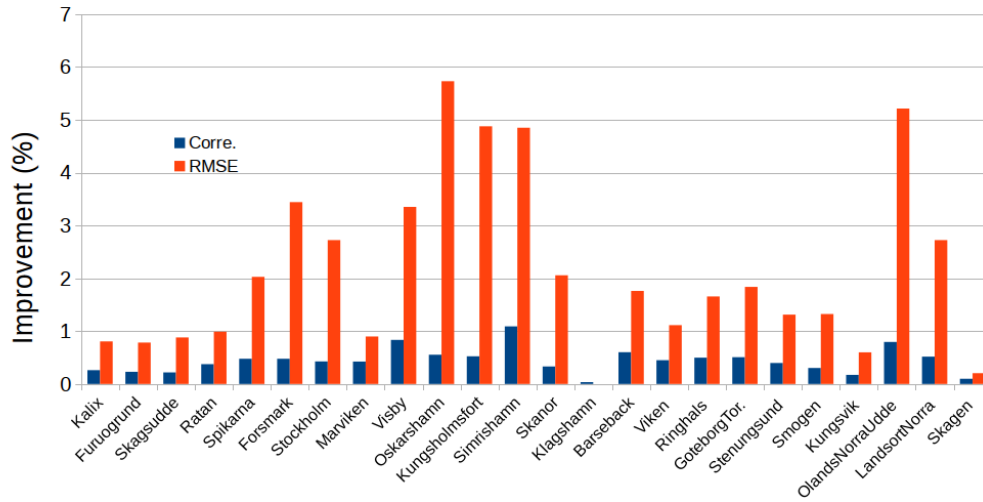
877 Figure 9. The overall RMSE and bias of temperature (up panel) and salinity (down panel) from FREE  
878 and ASSIM relative to observations as a function of water depth inside (b,d) and outside (a,c) of the  
879 Baltic Sea.

880

881

882

883



884

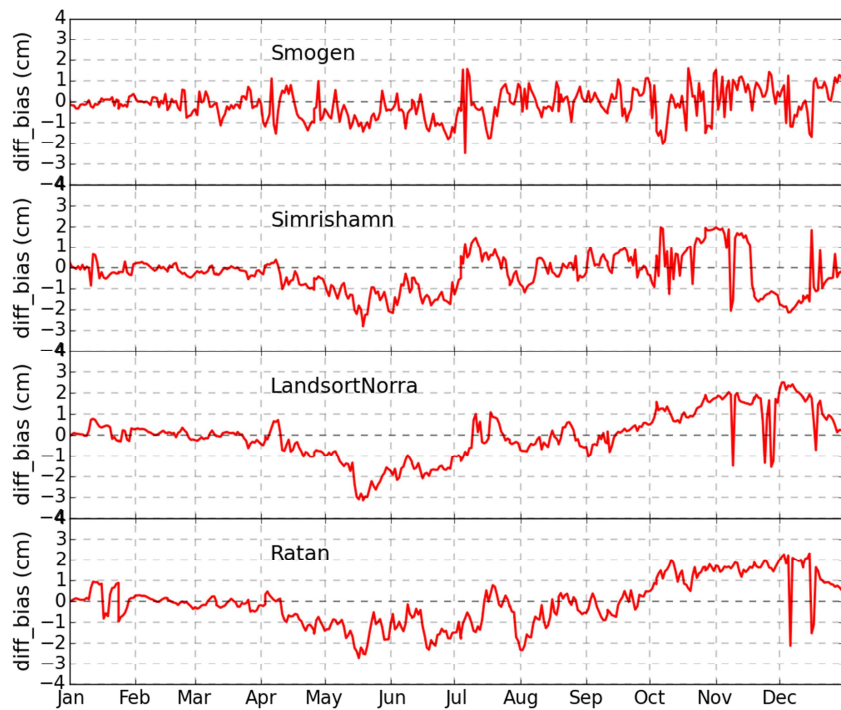
885 [Figure 10. The improvement \(%\) of correlation and RMSE for the SLA at the tide gauges stations. The](#)  
886 [station position is in the Figure 8b.](#)

887

888

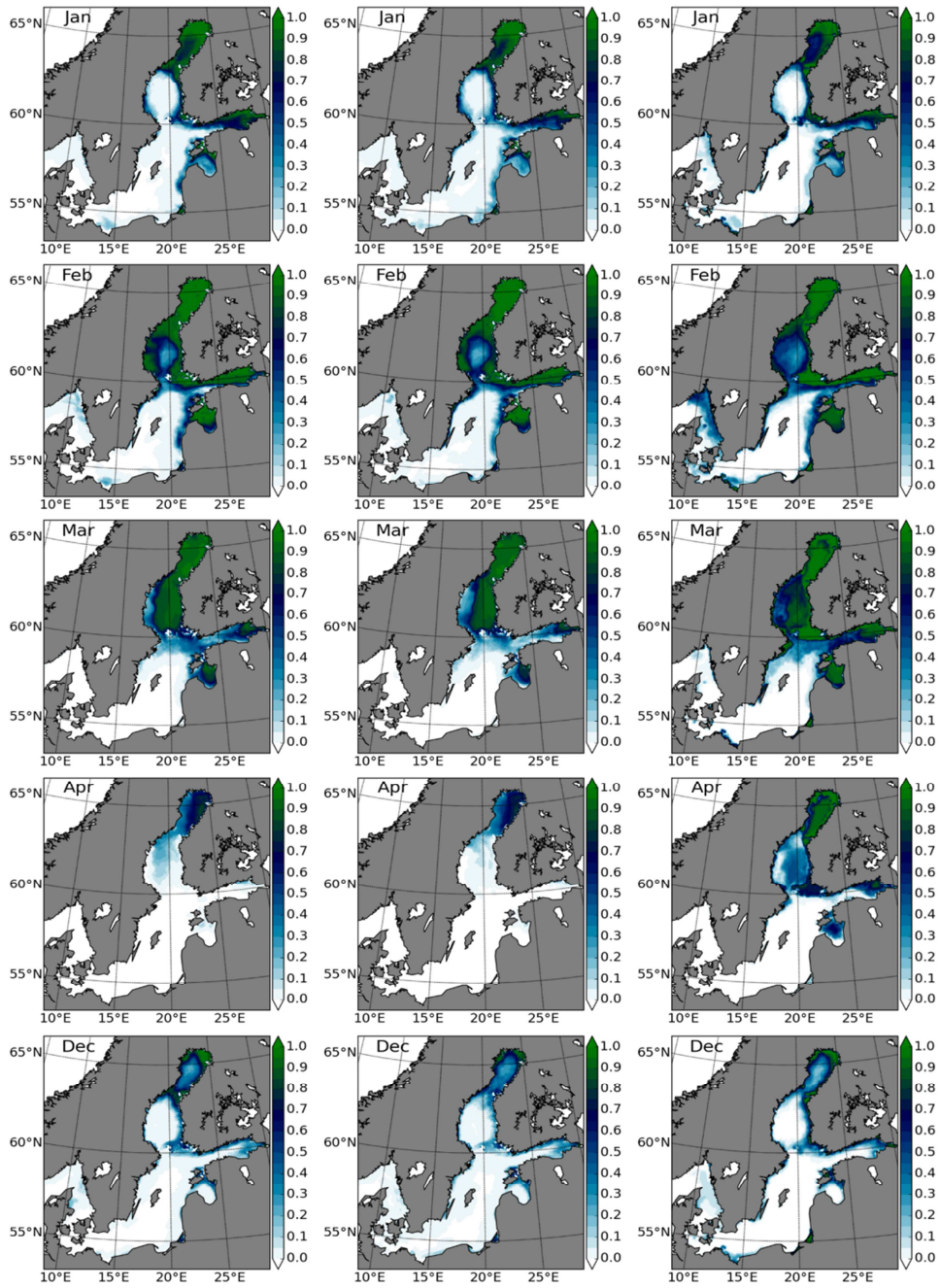
889

890



891  
 892 Figure 11. The [variation of SLA biases in ASSIM relative to FREE against](#) observations as a function  
 893 of time. The [station](#) position is [shown](#) in the [Figure 8b](#).

894  
 895  
 896  
 897



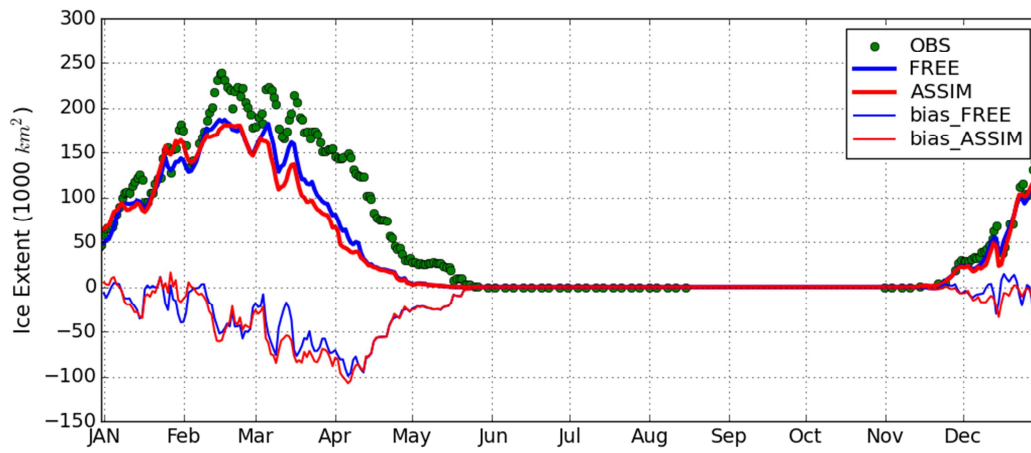
898

899 | Figure 12. The monthly mean sea ice concentrations in FREE (left panel), ASSIM (middle panel) and  
 900 | IceMap (right panel), respectively.

901

902

903



904

905 [Figure 13. The daily sea ice extent from FREE, ASSIM and IceMap and the sea ice extent bias \(mod-](#)  
 906 [elled minus observed field\), respectively.](#)

907